Inhibition of spikes in an array of coupled FitzHugh–Nagumo oscillators by means of alternating current

Arūnas Tamaševičius, Gytis Mykolaitis, Elena Adomaitienė, and Skaidra Bumelienė

***Abstract*—**Damping of spikes in an array of coupled oscillators by injection of sinusoidal current is studied both experimentally and numerically. The effect is investigated using an array, consisting of thirty mean-field coupled FitzHugh–Nagumo type oscillators. The results are considered as a possible mechanism of the deep brain stimulation, used to avoid the symptoms of the Parkinson's disease.

***Keywords*—**Alternating current, arrays of coupled oscillators, control of oscillations, FitzHugh–Nagumo oscillators.

I. Introduction

UNDESIRABLE instabilities in dynamical systems can be avoided by applying conventional proportional feedback techniques [1, 2]. An example is a simple second order system, where the proportional feedback is given by a linear term with a control coefficient k:

$$\begin{aligned} \dot{x} &= F(x,y) + k(x^* - x), \\ \dot{y} &= G(x,y). \end{aligned} \tag{1}$$

Here $F(\cdot)$ and $G(\cdot)$ are either linear or nonlinear functions, the x^* is a reference point, e.g. a steady state coordinate of the system. However, in many real systems, especially in biology, chemistry, physiology, etc., the exact locations of these states are unknown. Moreover, their positions may vary with time because of unknown and unpredictable forces. Therefore adaptive methods, automatically tracing and stabilizing the steady states are required. A large number of adaptive control techniques have been developed so far, e.g. the tracking filter method [3, 4], and applied to a variety of dynamical systems. To implement the tracking filter technique (1) should be provided with an additional equation, describing the dynamical variable z of the first order filter:

$$\begin{aligned} \dot{x} &= F(x,y) + k(z - x), \\ \dot{y} &= G(x,y), \\ \dot{z} &= \omega_f (x - z), \end{aligned} \tag{2}$$

where ω_f is the cut-off frequency of the filter (usually $\omega_f << 1$).

An alternative control method is a non-feedback technique based on applying to the system external periodic force:

$$\begin{aligned} \dot{x} &= F(x,y) + A\sin(\omega t), \\ \dot{y} &= G(x,y). \end{aligned} \tag{3}$$

In (3) the frequency of the external forcing ω should be high enough in comparison of the natural frequency of the uncontrolled dynamical system. A specific example is the stabilization of the unstable upside-down position of a mechanical pendulum by vibrating its pivot up and down at a relatively high frequency [5]. Recently [6] this "mechanical" idea has been exploited in a seemingly unexpected field, namely to get insight into the mechanism of the so-called deep brain stimulation (DBS), conventionally used to avoid tremor for patients with the Parkinson's disease.

In this paper, we extend this research by demonstrating that external periodic forcing can inhibit spikes in an array of coupled neuronal oscillators. To be specific, we consider an array of the mean-field coupled electronic FitzHugh–Nagumo (FHN) oscillators, also known in literature as the Bonhoeffer–van der Pol oscillators.

II. Electrical Circuits

The corresponding circuit diagrams are presented in Fig. 1. In Fig. 1(a) CN is a coupling node. It is assumed, that the CN is not accessible directly from the outside, but via some passive resistance network, represented here for simplicity by an equivalent resistance R_g. DN is an accessible damping node.

In Fig. 1(b) OA is a general-purpose operational amplifier, e.g. NE5534 type device, D_1 and D_2 are the BAV99 type Schottky diodes, $L = 10$ mH, $C = 3.3$ nF, $R_1 = R_2 = 1$ kΩ, $R_3 = 510$ Ω, $R_4 = 30$ Ω, $R_5 = 510$ Ω, $R_6 = 275$ Ω (an external resistor $R_6' = 220$ Ω in series with the coil resistance $R_6'' = 55$ Ω), $R_{7i} = (24+i)$ kΩ, $i = 1, 2, \ldots N$, $R^* = 510$ Ω, $V_0 = -15$ V.

A. Tamaševičius (corresponding author, phone: 370-671-93904; fax: 370-5-262-7123; e-mail: tamasev@pfi.lt), E. Adomaitienė (e-mail: elena.tamaseviciute@ftmc.lt), and S. Bumelienė (e-mail: skaidra@pfi.lt) are with the Department of Electronics, Center for Physical Sciences and Technology, 11 A. Goštauto str., LT-01108 Vilnius, Lithuania.

G. Mykolaitis is with the Department of Physics, Faculty of Fundamental Sciences, Vilnius Gediminas Technical University, 11 Saulėtekio al., LT-10223 Vilnius, Lithuania (e-mail: gytis@pfi.lt).

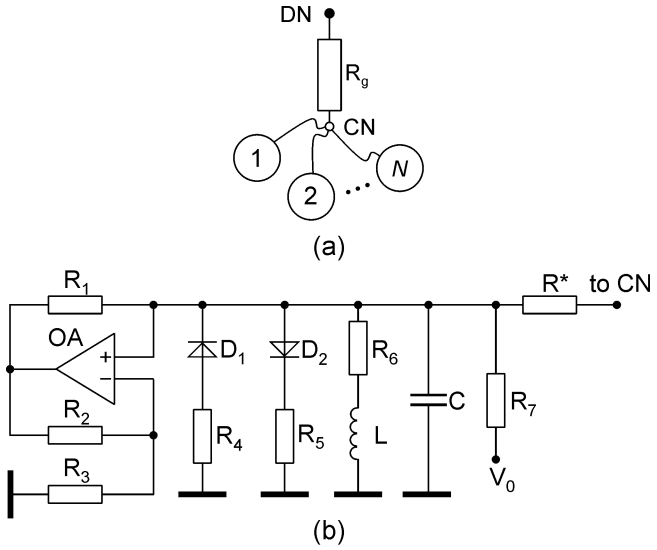

Fig. 1 Circuit diagrams. (a) array of mean-field coupled oscillators, (b) single asymmetric ($R_4 << R_5$) FHN type oscillator

The single FHN oscillator in Fig. 1(b) is a circuit with an *asymmetric* nonlinearity ($R_4 << R_5$). It is a slight modification of an oscillator, described in [7] and essentially differs from the earlier asymmetric version of the FHN type oscillator, suggested in [8].

In the experiments we employed a hardware array with $N = 30$, described in details (without any external control) elsewhere [9].

III. Experimental Results

The external inhibitory AC current $I_{inh}(t) = I_A \sin(2\pi f t)$ was injected from an external sine wave generator via the damping node DN. For the best performance it is necessary to choose an appropriate drive amplitude I_A and frequency f. The f should be much higher than the natural frequency f_0 of the spiking oscillators ($f_0 \approx 12$ kHz). The experimental results are shown in Fig. 2 and Fig. 3, by the waveforms and the phase portraits (in classical electronics called the Lissajous figures). Here the $<V_C>$ is the mean-field voltage of the voltages V_{Ci} from the individual oscillators ($i = 1, 2 \ldots 30$). The threshold amplitude of the inhibitory current is $I^*_A = 50$ mA, the optimal frequency is $f \approx 150$ kHz, providing the lowest threshold.

The time average of the high frequency non-spiking voltage $<V_C>$ (right hand side of the bottom plot), taken over the period ($T = 1/f$) of the external current, is $\bar{U}_C \approx -0.18$ V. It is non-zero value because of the DC bias $V_0 = -15$ V. The $\bar{U}_C$ is noticeably different from the natural steady state $<V_{0C}> = -0.27$ V, measured in a non-oscillatory mode (when the all coils L are short-circuited).

Fine diagonals in Fig. 3, $[V_{C30}, <V_C>]$ indicate, that the individual oscillator #30 is strongly synchronized with the mean-field of the array. Other oscillators, #1 to #29 were also checked experimentally by means of the phase portraits $[V_{Ci}, <V_C>]$ and gave similar result.

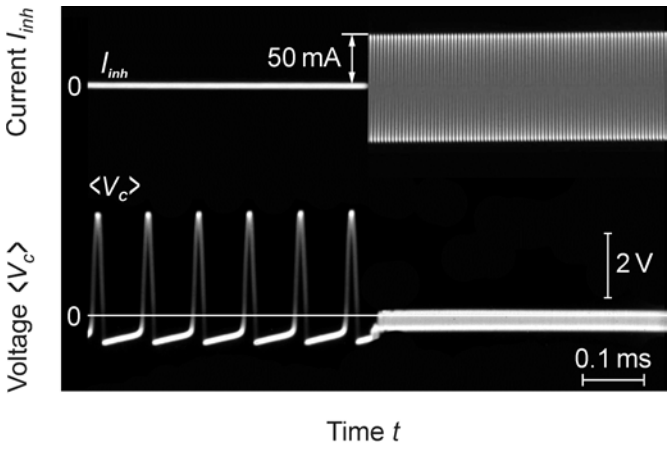

Fig. 2 Experimental waveforms of the external periodic current I_{inh} and the mean-field voltage of the array $<V_C>$. $f = 150$ kHz

Evidently, the self-sustained low frequency ($f_0 \approx 12$ kHz) spikes of about 4 V height are totally suppressed, when the inhibitory current $I_A \geq I_A^* = 50$ mA is injected. However, we have a finite (≈ 10%) higher frequency artefact. The voltage oscillates around the time average $\bar{U}_C$ with the amplitude of about 0.4 V at the external drive frequency f.

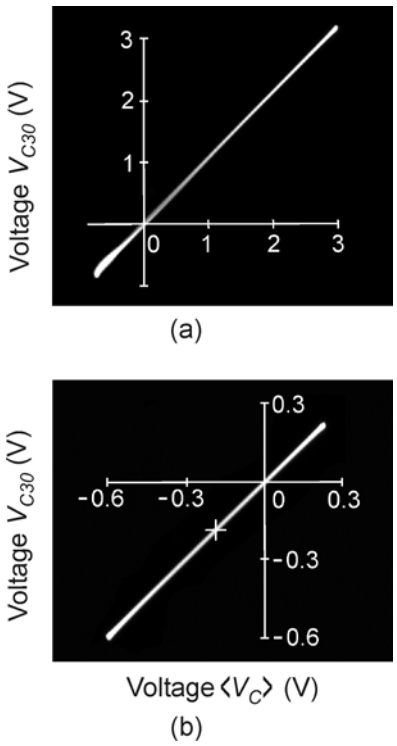

Fig. 3 Phase portraits $[V_{C30}, <V_C>]$. (a) Spiking oscillators (no control, $I_A = 0$), (b) Non-spiking oscillators, $I_A = 50$ mA, $f = 150$ kHz. Small cross in (b) marks the averages of the voltages $[\bar{U}_{C30}, \bar{U}_C]$ taken over the period of the external inhibitory current $I_{inh}(t)$. They are at about [−0.18 V, −0.18 V]. Note different position of the diagonal also different horizontal and vertical scales in (b), compared to (a)

Moreover, the artefact voltage continues to change (Fig. 4), when the external drive amplitude I_A is increased above the threshold value I^*_A (the amplitude I_A should be somewhat higher than the threshold to guarantee robust inhibition). For example, at a double drive amplitude, $I_A/I_A^* = 2$ the average voltage changes its sign. Similar behavior was observed earlier, but not emphasized, in the numerically simulated bifurcation diagram for the Hodgkin–Huxley (HH) single neuron model [6].

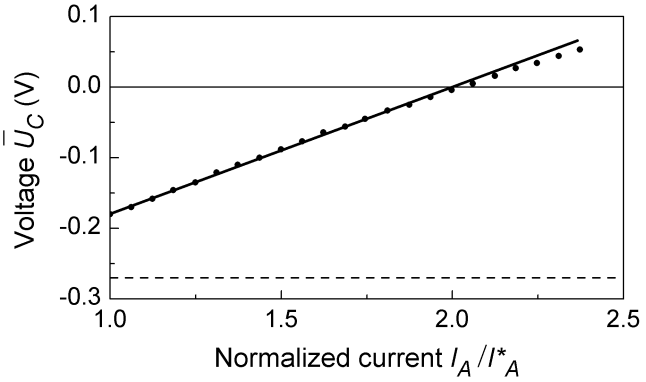

Fig. 4 Time average of the mean-field voltage $\bar{U}_C$, taken over the period ($T = 1/f$) of the external inhibitory current I_{inh}, as a function of the normalized amplitude I_A/I_A^* of the external current. $I_A^* = 50$ mA. Extrapolation to zero control ($I_A = 0$) provides a value of $\bar{U}_C$ close to the natural steady state $\langle V_{0C} \rangle = -0.27$ V (dashed line in the plot)

IV. Mathematical Model

Applying the Kirchhoff's laws to the circuits in Fig. 1 with $R_1 = R_2$ and $R_7 >> \max((L/C)^{1/2}, R_3, R_4, R_5, R_6)$ the following differential equations are derived:

$$C\frac{dV_{Ci}}{dt} = \frac{V_{Ci}}{R_3} - I_D - I_{Li} + \frac{V_0}{R_{7i}} + \frac{\langle V_C \rangle - V_{Ci}}{R^*} + \frac{I_A \sin(2\pi f t)}{N},$$
$$L\frac{dI_{Li}}{dt} = V_{Ci} - R_6 I_{Li}, \quad i = 1, 2 \ldots N. \tag{4}$$

The nonlinear current-voltage (I-V) characteristic $I_D = I_D(V_{Ci})$ of the D_1R_4–D_2R_5 composite in (4) is approximated by three segments of linear functions

$$I_D(V_{Ci}) = \begin{cases} (V_{Ci} + V^*)/R_4 & , \quad V_{Ci} < -V^*, \\ 0 & , \quad -V^* \le V_{Ci} \le V^*, \\ (V_{Ci} - V^*)/R_5 & , \quad V_{Ci} > V^*. \end{cases} \tag{5}$$

Here V^* is the "breakpoint" voltage of the forward I-V characteristic of the diodes ($V^* \approx 0.6$ V). In (4) the individual oscillators are coupled via the mean-field voltage

$$\langle V_C \rangle = \frac{1}{N}\sum_{i=1}^{N} V_{Ci} \,. \tag{6}$$

By introducing the following set of dimensionless variables and parameters:

$$x_i = \frac{V_{Ci}}{V^*}, \quad y_i = \frac{\rho I_{Li}}{V^*}, \quad t \to \frac{t}{\sqrt{LC}},$$
$$\langle x \rangle = \frac{1}{N}\sum_{i=1}^{N} x_i, \quad \rho = \sqrt{L/C},$$
$$a = \frac{\rho}{R_3}, \quad b = \frac{R_6}{\rho}, \quad c_i = \frac{\rho}{R_{7i}} \cdot \frac{V_0}{V^*}, \tag{7}$$
$$d_1 = \frac{\rho}{R_4}, \quad d_2 = \frac{\rho}{R_5}, \quad k = \frac{\rho}{R^*}, \quad i = 1, 2, \ldots N$$

also two additional dimensionless parameters for the external sine wave forcing:

$$A = \frac{\rho I_A}{N V^*}, \quad \omega = 2\pi f \sqrt{LC} \tag{8}$$

we arrive to a set of $2N$ coupled non-autonomous differential equations, convenient for numerical integration:

$$\dot{x}_i = a x_i - f(x_i) - y_i + c_i + k(\langle x \rangle - x_i) + A \sin \omega t,$$
$$\dot{y}_i = x_i - b y_i, \quad i = 1, 2, \ldots N. \tag{9}$$

The $f(x_i)$ in (9) is a nonlinear function, presented by a piecewise linear function

$$f(x_i) = \begin{cases} d_1(x_i + 1) & , \quad x_i < -1, \\ 0 & , \quad -1 \le x_i \le 1, \\ d_2(x_i - 1) & , \quad x_i > 1. \end{cases} \tag{10}$$

Note, that due to $d_1 >> d_2$ the $f(x_i)$ is an essentially asymmetric function [7] in contrast to the common FHN cubic parabola x^3, introduced by FitzHugh [10]. The DC bias parameters c_i are intentionally set different for each individual oscillator, thus making them non-identical units.

V. Numerical Results

Integration of (9) has been performed using the Wolfram MATHEMATICA package. The numerical results are presented in Fig. 5. They are in a good agreement with the experimental plots in Fig. 2. The mean-field variable $\langle x_i \rangle$ does not converge to a constant steady state, but oscillates around it at the drive frequency. Strictly speaking, the non-autonomous (externally driven) dynamical systems, e.g. given by (9), do not possess steady states at all. Only in the case of high frequency ($f >> f_0$) drive we can introduce the average values, taken over the external period. These averages more or less are related to the steady states.

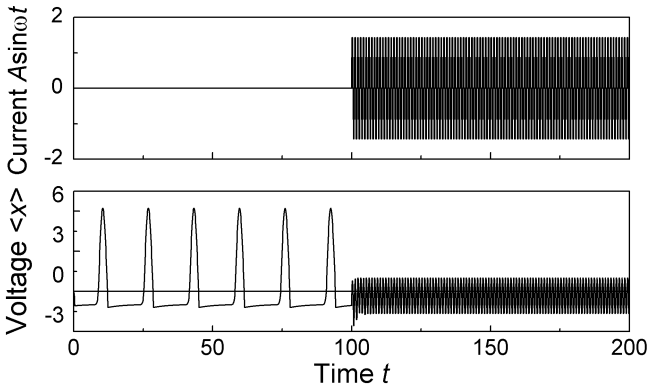

Fig. 5 Simulated waveforms of the inhibitory current $A\sin(\omega t)$ and the mean-field voltage $\langle x \rangle$ from (9, 10), $N = 30$. $A = 5.1$, $\omega = 6.28$, $a = 3.4$, $b = 0.16$, $c_i = -44/(24 + i)$, $i = 1, 2, \ldots 30$, $d_1 = 60$, $d_2 = 3.4$, $k = 3.4$. The external inhibitory term $A\sin(\omega t)$ is activated at $t = 100$

VI. Mean-Field Approach and Linear Analysis

Analysis of (9) can be essentially simplified, if we consider the mean-field variables only, obtained by direct averaging the x_i, y_i, $f(x_i)$, and c_i in the original equations:

$$\begin{aligned} \langle \dot{x} \rangle &= a\langle x \rangle - \langle f(x) \rangle + \langle y \rangle + \langle c \rangle + A\sin \omega t, \\ \langle \dot{y} \rangle &= \langle x \rangle - b\langle y \rangle. \end{aligned} \tag{11}$$

As a result, the coupling term $k(\ldots)$ in (11) has been nullified independently on the value of k. Further we assume, that all $|x_i| \le 1$. According to (10) this leads to $f(x_i) = 0$. Eventually we obtain a set of linear differential equations, which does not describe the full dynamics of the mean field, but provides its steady state. In the absence of the external drive ($A = 0$) it has the following coordinates (for $ab < 1$ and $|c_i| \le 1/b–a$):

$$\langle x_0 \rangle = b\langle c \rangle/(1-ab), \quad \langle y_0 \rangle = \langle c \rangle/(1-ab). \tag{12}$$

Stability analysis of (11) shows, that for and $a > b$ the steady state, given by (12), is unstable (the real parts of the both eigenvalues of the corresponding second order characteristic equation are both positive). If (in addition to $a > b$) the sum $a + b > 2$, then the eigenvalues are real (no imaginary parts). Thus, the steady state (12) is an unstable node. Whereas the external periodic forcing ($A \ne 0$), similarly to the mechanical pendulum [5], can stabilize the originally unstable steady state.

For the set of the parameter values, employed in numerical simulations: $a = 3.4$, $b = 0.16$, and $c_i = -44/(24+i)$, the steady-state coordinates, given by (12), have the following numerical values: $\langle x_0 \rangle = -0.41$, $\langle y_0 \rangle = -2.57$. Using the definitions of the dimensionless variables, introduced in (7), we estimate the means of the steady-state coordinates of the original system: $\langle V_{0C} \rangle \approx -0.25\,\text{V}$, $\langle I_{0L} \rangle \approx -1\,\text{mA}$. The estimated steady-state voltage is close to its experimental value –0.27 V.

VII. Conclusion

In the recent theoretical papers on suppression of neuronal spikes by means of alternating current, the mathematical models of *single* neurons have been considered, the HH [6] and the FHN [11] models, respectively. Our earlier paper [7] on the adaptive feedback technique, suggested to damp spiking FHN type neurons also deals with a *single* oscillator only. In contrast to the above papers, in the present work we have investigated an *array* of coupled FHN type neuronal oscillators. Moreover, using an analogue electronic network we have carried out an imitative experiment. It can serve for better understanding the DBS technique, used to suppress the symptoms of the Parkinson's disease.

The influence of the strongly perturbed steady states of the neurons on the treatment by means of the DBS technique [12] has not been investigated yet. However, one can intuitively suppose, that the high frequency artefact oscillations, observed in the "electronic" experiment (Fig. 2) due to injection of the alternating current into an array of oscillators and especially its unnatural DC component (Fig. 4) can indicate the reason of undesirable side effects in the real neuronal cells.

References

[1] B. C. Kuo, *Automatic Control Systems*. Englewood Cliffs, New Jersey: Prentice Hall, 1995.

[2] K. Ogata, *Modern Control Engineering*. Englewood Cliffs, New Jersey: Prentice Hall, 2010.

[3] N. F. Rulkov, L. S. Tsimring, and H. D. I. Abarbanel, "Tracking unstable orbits in chaos using dissipative feedback control," *Phys. Rev. E*, vol. 50, pp. 314-324, 1994.

[4] A. Namajūnas, K. Pyragas, and A. Tamaševičius, "Analog techniques for modeling and controlling the Mackey–Glass system," *Int. J. Bifurcation Chaos*, vol. 7, no.4, pp. 957–962, 1997.

[5] J. J. Thomsen, Vibrations and Stability – Advanced Theory, Analysis and Tools. Berlin, Heidelberg, New York: Springer-Verlag, 2003.

[6] K. Pyragas, V. Novičenko, and P. A. Tass, "Mechanism of suppression sustained neuronal spiking under high-frequency stimulation," *Biol. Cybern.*, vol. 107, pp. 669-684, 2013.

[7] A. Tamaševičius, E. Tamaševičiūtė, G. Mykolaitis, S. Bumelienė, R. Kirvaitis, and R. Stoop, "Neural spike suppression by adaptive control of an unknown steady state," in *Proc. 19th Int. Conf. Artificial Neural Networks*, Limassol, Cyprus, September 2009; *Lecture Notes Comp. Sci.*, vol. 5768, pp. 618–627, 2009.

[8] S. Binczak, V. B. Kazantsev, V. I. Nekorkin, and J. M. Bilbaut, "Experimental study of bifurcations in modified FitzHugh-Nagumo cell," *Electron. Lett.*, vol. 39, no. 13, pp. 961–962, 2003.

[9] E. Tamaševičiūtė, G. Mykolaitis, and A. Tamaševičius, "Analogue modelling an array of the FitzHugh–Nagumo oscillators," *Nonlinear Analysis: Modelling and Control*, 2012, vol 17, no. 1, pp. 118–125, 2012. Available: http://www.mii.lt/na

[10] R. FitzHugh, "Impulses and physiological states in theoretical models of nerve membrane," *Biophys. J.*, vol. 1, no. 6, pp. 445–466, 1961.

[11] A. Rabinovitch, Y. Biton, D. Braunstein, M. Friedman, and I. Aviram, "A neuron under external sinusoidal stimulation," *Brain Stimul.*, vol. 8, pp. 310-325, 2015.

[12] A. L. Benabid, S. Chabardes, J. Mitrofanis, and P. Polak, "Deep brain stimulation of the subthalamic nucleus for the treatment of Parkinson's disease," *Lancet Neurol.*, vol. 8, no. 1, pp. 67–81, 2009.

Development of a temperature and heat insensitive lathe via neural network inverse analysis control

Ikuo TANABE

Abstract— Since the beginning of the 21st century, the importance to manufacture products in an environmentally-conscious way has been highlighted. In this regard, manufacturers not only need to conserve energy, but they also need to scrutinize in order to save resources and reduce environmentally-harmful pollutants. Nevertheless, most machine tools highly depend on lubricating oil to achieve a smoother drive, large amounts of electricity during forced cooling to attain a high accuracy, as well as large amounts of cutting oil to accomplish lubrication and cooling effects. Since this represents a large environmental problem, a lathe insensitive to temperature and heat fluctuations was developed and evaluated. Specifically, the developed lathe was meant to be both a three-dimensional fixed-zero system structure and a forced self-cooling structure. Furthermore, an air flow speed control used on the forced self-cooling system was developed, using the neural network inverse analysis, for the reduction of thermal deformation on the bench lathe. Thereafter, the thermal deformation of the developed lathe present in several experiments was measured and evaluated. As a result it is concluded that: (1) even though there was no active forced cooling, the thermal deformation of the bench lathe was considerably small, and (2) the air flow speed control used on the forced self-cooling system, through the neural network inverse analysis, was effective in achieving a stable operation, disregarding weather variations.

***Keywords*—** Forced Cooling, Machine Tool, High Accuracy, Neural Network Inverse Analysis, Cutting.

I. Introduction

As the industry demands an ever-growing high-precision manufacturing, the importance to reduce the thermal deformation on machine tools has been underlined. Nowadays, many studies regarding the thermal deformation on machine tools had been made [1], [2]; among these are: forced cooling of the main spindle or ball screws [3], [4], [5], [6], control of the thermal expansion feedback, heat-insulation of the heat source [7], and so forth.

I. TANABE is with the Nagaoka University of Technology, Dept. of Mechanical Engineering, 1603-1 Kamitomioka, Nagaoka, Niigata, 940-2188, JAPAN (phone: 0081-258-47-9727; fax: 0018-258-47-9770; e-mail: tanabe@mech.nagaokaut.ac.jp).

However, in the case of the forced cooling of the main spindle, the control to reduce the machine tool thermal deformation has proven to be difficult. This is because there are many non-linear factors in the machine tool thermal deformation process, such as an irregular room-temperature fluctuation, thermal dependence of a certain material, fluctuations on the preload of the spindle bearing, etc.

Therefore, a new lathe insensitive to temperature and heat fluctuations was developed. In addition, an air flow speed control used on the forced self-cooling system was developed, using the neural network inverse analysis [8], for the reduction of thermal deformation on the bench lathe. Thereafter, a control method for the thermal deformation of the developed lathe was evaluated through several experiments.

II. Development of a Lathe Incorporating Heat Countermeasures [9]

A. Three-dimensional fixed-zero system structure

As shown in Fig. 1, the design of this new structure is meant to have thermal deformation but none of the effects. This is because the machining point of the lathe is continually changing in the X, Y, Z axes in respect of the origin of the thermal deformation. Thus, just by using this countermeasure related to the machine tool structure, the thermal deformation effect is effectively reduced to achieve a high-accuracy machining.

B. Forced self-cooling structure

As shown in Fig. 2, the design of this structure is meant to perform a forced cooling through the vaporization of cooling water. Specifically, considering a steady water supply and the capillary action of water, this is achieved by attaching a water-soaked cloth to the machine tool surface. Moreover, three fins are attached to the lathe chuck in order to blow a strong air flow. Consequently, the machine tool heat is removed through the water vaporization process and, as a result, the machine tool thermal deformation is reduced. Given that the headstock front surface is a large heat source during machining and that a strong air flow can be generated through the spindle rotation, it was considered that this area was the optimum place to attach the cloth. Particularly, when the spindle rotation increases, the internal heat generation becomes more intense. Correspondingly, the air flow becomes stronger and the surface is cooled down at a large heat transfer rate.

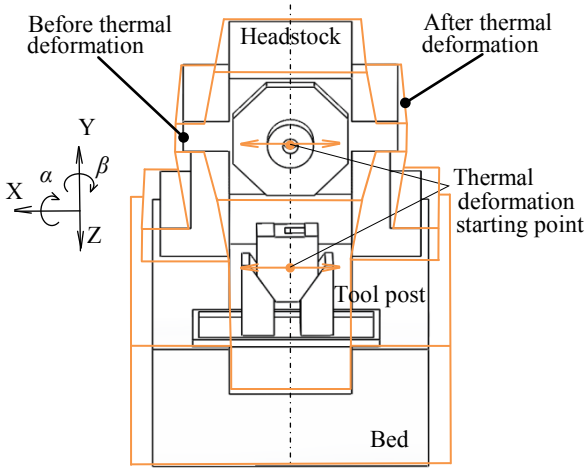

(a) X-axis fixed-zero displacement

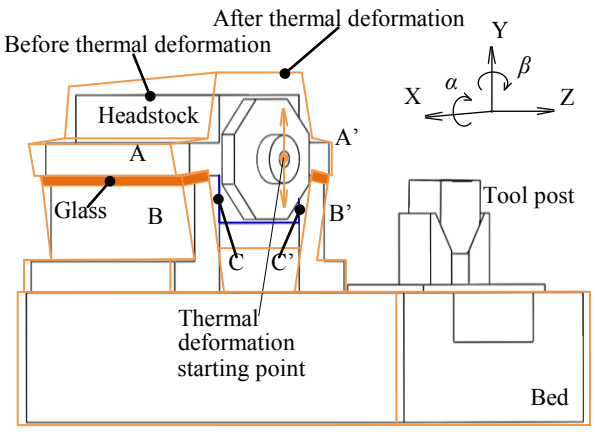

(b) Y-axis fixed-zero displacement

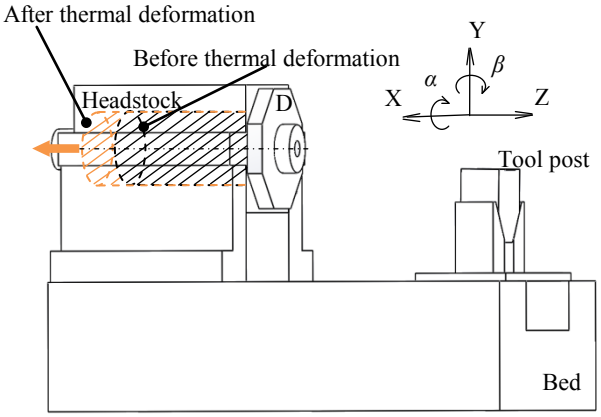

(c) Z-axis fixed-zero displacement

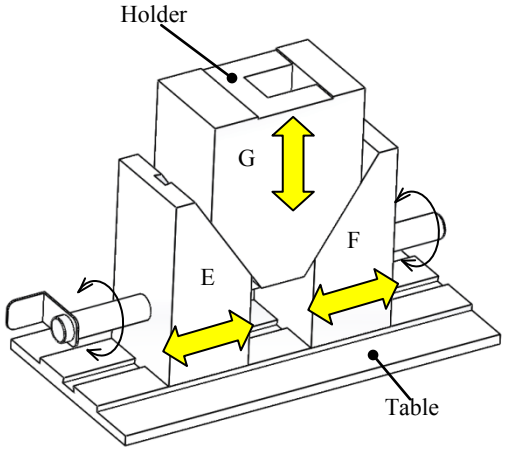

(d) Adopted tool post mechanism

Fig. 1 Schematic view of the three-dimensional fixed-zero system structure for the thermal influence reduction

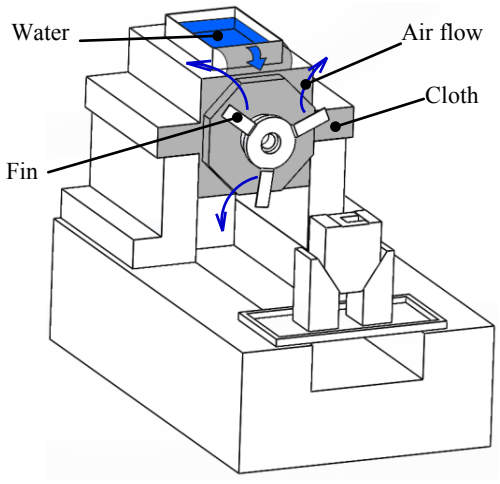

Fig.2 Schematic view of the forced self-cooling structure

Subsequently, the air flow speed control used on the forced self-cooling system was developed. In this case, given that neural networks are suitable for the management of non-linear phenomena, the neural network inverse analysis was used to estimate the optimum angles of the lathe chuck fins.

III. Neural Network Inverse Analysis

A. *Neural network of the lathe thermal deformation*

In this section, a newly developed method to analyze the lathe thermal deformation using the neural network inverse analysis will be explained [10]. Firstly, the multiple variables in the neural network will be explained. In this regard, the bench lathe used in this experiment was the one developed in the previous section and the experimental setup for it is shown in Fig. 3. In particular, the experimental setup consisted of T-type thermocouples for the retrieval of data, regarding the structural temperature and the room-temperature, that could be processed as training data of the neural network. Similarly, spindle speed, humidity, fin angle and the thermal behavior in the X, Y and Z axes were measured and treated as training data; in the case of thermal behavior, dial gauges were used for measurement.

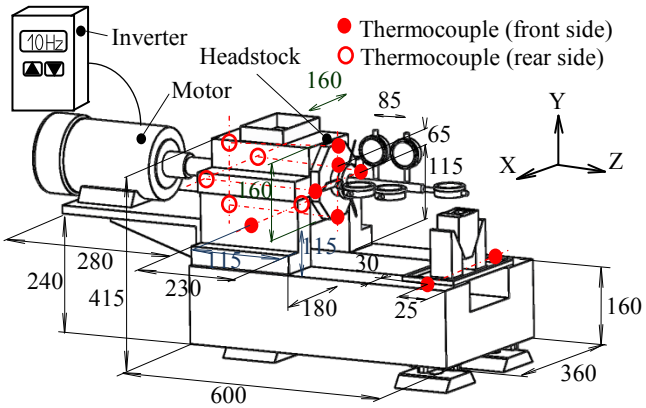

Fig. 3 Bench lathe experimental setup

Table 1 Specifications of the bench lathe used for experimentation

Head stock	Center height (from bed top)	177 mm
	Center height (from floor)	337 mm
	Spindle speed	Max.3600 min^{-1}
	Front bearing	50BNC10TYDBB
	Rear bearing	45BN10TYDB
Bed	Dimensions	600×360×160 mm
Tool post	Y-axis stroke	30 mm
Table	Z-axis stroke	200 mm
Motor	Power	0.75 kW
	Speed	Inverter control
Total weight		200 kg

Table 2 Experimental parameters used for the neural network construction

Recreated weather conditions	Fine, Overcast, Rainy
Forced self-cooling system fin angle (deg.)	η= 30, 60, 90
Spindle speed (min^{-1})	Case A, Case B, Case C

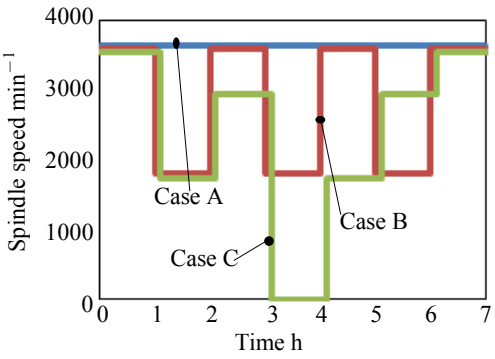

Fig. 4 Evaluated spindle speed cases during experimentation

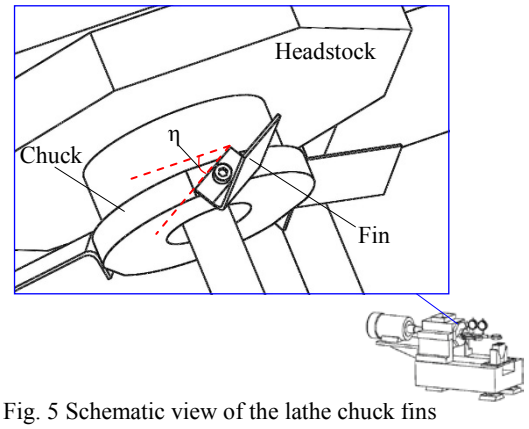

Fig. 5 Schematic view of the lathe chuck fins

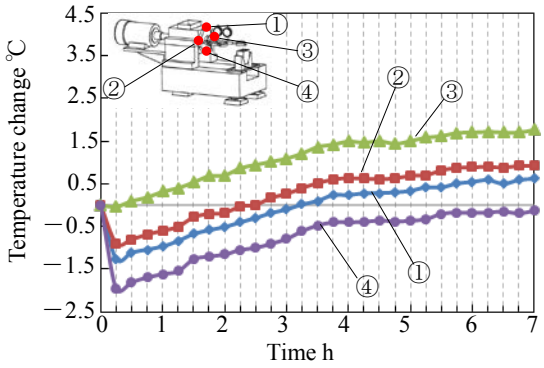

Fig. 6 Bench lathe thermal behavior experimental results

Specifications of the bench lathe used for experimentation are shown in Table 1. Additionally, the experimental parameters used for constructing the neural network are shown in Table 2. In this regard, in order to appreciate its effect, parameters were manipulated so the weather conditions on a fine day, an overcast day and a rainy day are recreated. Moreover, three angle patterns for the forced cooling control fins were used: 30, 60 and 90 degrees.

Furthermore, as shown in Fig. 4, spindle rotation speeds were set in three different patterns: Case A, Case B and Case C. Subsequently, the bench lathe chuck fins angle is defined as angle η as shown in Fig. 5. In particular, the angle of the fins is manipulated to control the air flow over the cloth during operation (see Fig. 2) and restrain the thermal deformation of the machine tool. After this, the heat of vaporization, the vaporization fluctuation and the cloth heat transfer coefficient were changed in order to ultimately achieve the cooling of the bench lathe and the reduction of the thermal deformation. To illustrate, the experimental results of the bench lathe thermal behavior are shown in Fig. 6. Prior to this, the experimental setup consisted of a recreated fine weather, a 60 degrees fin angle, a 3600 min^{-1} spindle speed and a no-cutting idling state; data retrieval was done every 15 minutes for a 7 hours period. Thus, 29 data units were retrieved from one experiment and used as training data for the neural network. It is necessary to mention that all the experiments were performed under the same procedure. For this experiment, since it has a strong non-linear

mapping ability during the training of a neural network, a three-layer backpropagation method was used. In this regard, the bench lathe neural network model is shown in Fig. 7. Specifically, the number of input layers is 33: a bench lathe working time t, spindle speed $N(t)$, 13 bench lathe structural temperatures $\theta_s(t)$, room-temperature $\theta_r(t)$, humidity $h(t)$ at working time t, 13 bench lathe structural temperature changes $\theta_s(t)-\theta_s(t-0.5)$, room-temperature fluctuation $\theta_r(t)-\theta_r(t-0.5)$, humidity fluctuation on a 30 minutes interval $h(t)-h(t-0.5)$, and fin angle $\eta(t)$ at working time t. Similarly, the number of hidden layers is 99, and the output layers are only the total deformation in the X, Y and Z axes.

In Fig. 7, W_{ij} are the linking weights between the input and the hidden layers, V_{jk} are the linking weights between the hidden and the output layers, while the offset values of the hidden and output layers are β_j and γ_k, respectively. In addition, a sigmoid function was used as the transform function in the hidden layer.

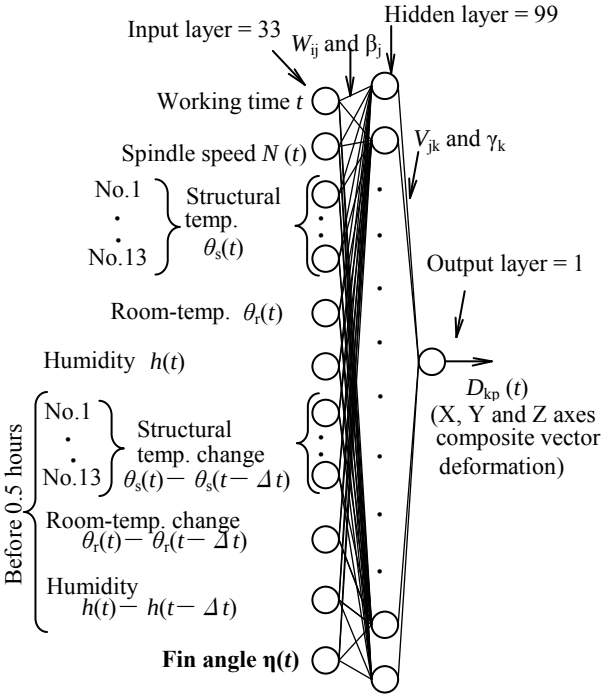

Fig.7 Neural network model between the measured temperatures, the forced self-cooling structure and the thermal deformation on the three-dimensional fixed-zero system structure.

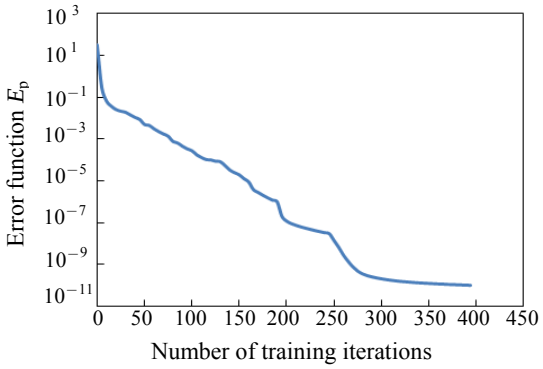

Fig. 8 Error convergence on the training process

Given that 29 training data units and 27 training patters were used, the amount of data sets was 783. In other words, 29 training units of measured data were used in each training pattern. In Fig. 8, the relationship between the number of training iterations and the error function can be appreciated. In this regard, the error function E_p is calculated using equation (1).

$$E_p = \frac{1}{2} \sum_k (T_{kp} - D_{kp})^2 \quad (1)$$

Where T_{kp} and D_{kp} are the training data and the output data of the unit k in the training pattern p; when the training iterations reached a 394 value and the error function converged to 9.97×10^{-11}, training iterations concluded. After the calculation, the neural network linking weights W_{ij}, V_{jk} and offset values β_j, γ_k were taken out for the inverse analysis.

B. Lathe control method through the neural network inverse analysis

Thereafter, the optimum fin angle $\eta_o(t)$ for the bench lathe chuck fins was calculated through the inverse analysis of this neural network. For this, the linking weights W_{ij}, V_{jk} and offset values β_j, γ_k in the neural network were used and an algebraic expression for the inverse analysis, and consequently for control of the optimum fin angle $\eta_o(t)$, was constructed. Furthermore, the relationship between the thermal deformation $D_{kp}(t)$ and the fin angle $\eta(t)$ followed equation (2).

$$D_{kp}(t) = f\{ W_{ji}, V_{kj}, \zeta_{jj}, \gamma_k, \theta_s(t), \theta_s(t-\Delta t), \theta_r(t), \theta_r(t-\Delta t), t, h(t), h(t-\Delta t), N(t), \eta, \}$$

$$= \sum_{p=1}^{99} \frac{V_{kp}}{1+\exp\{-\sum_{q=1}^{33}(W_{pq} \cdot I_q + \zeta_{jp})\}} + \gamma_k \quad (2)$$

Where

$$I_q = \begin{bmatrix} I_1 \\ I_2 \\ I_3 \\ \vdots \\ I_{33} \end{bmatrix} = \begin{bmatrix} t \\ \theta_s(t) \\ \theta_s(t-0.5) \\ \theta_r(t) \\ \theta_r(t-0.5) \\ h(t) \\ h(t-0.5) \\ \eta(t) \end{bmatrix}$$

Here, at working time t, the fin angle $\eta(t)$ and the thermal deformation $D_{kp}(t)$ are two unknown variables, while the other variables involved are considered as known. Through equation (2), and a feedforward control, it was possible to calculate the the optimum fin angle $\eta_o(t)$ to minimize the thermal deformation $D_{kp}(t)$.

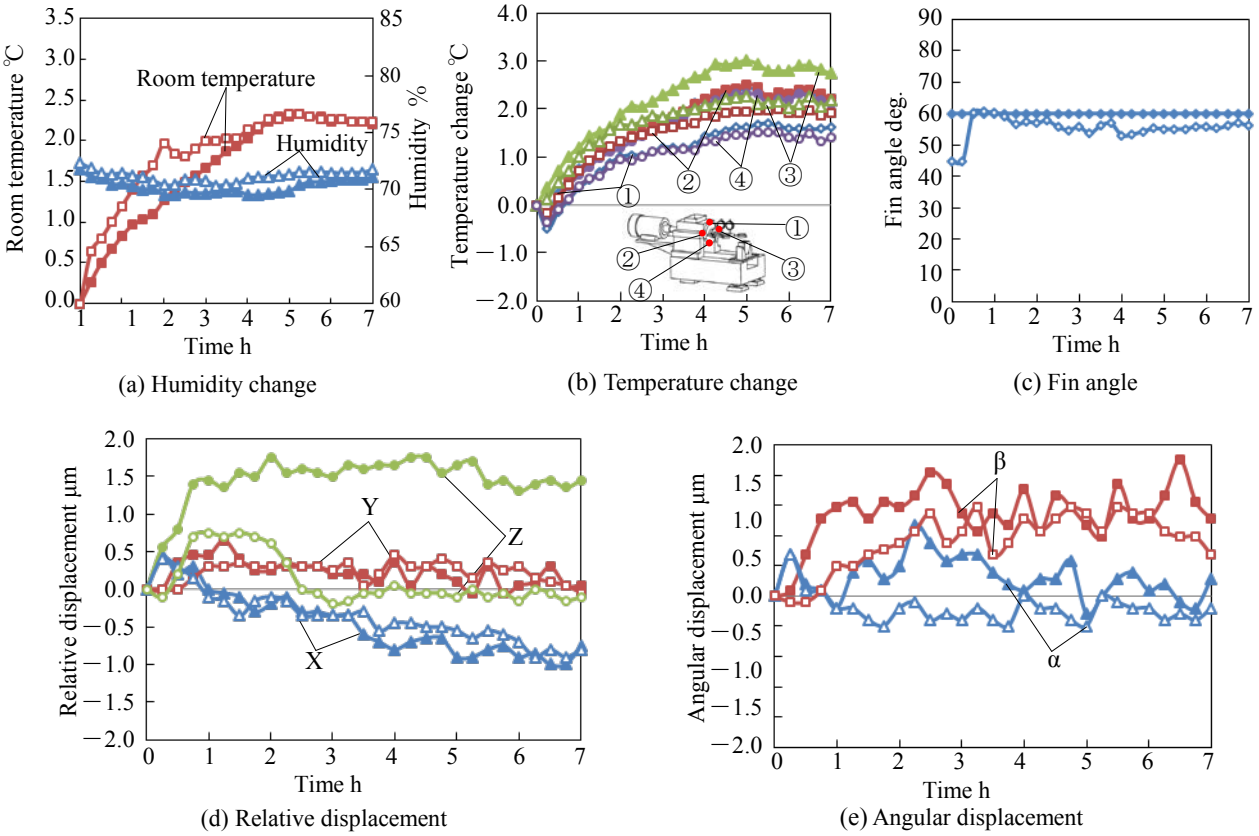

Fig.9 Bench lathe thermal deformation behavior under fine weather conditions
(filled markers: without the proposed system; empty markers: with the proposed system)

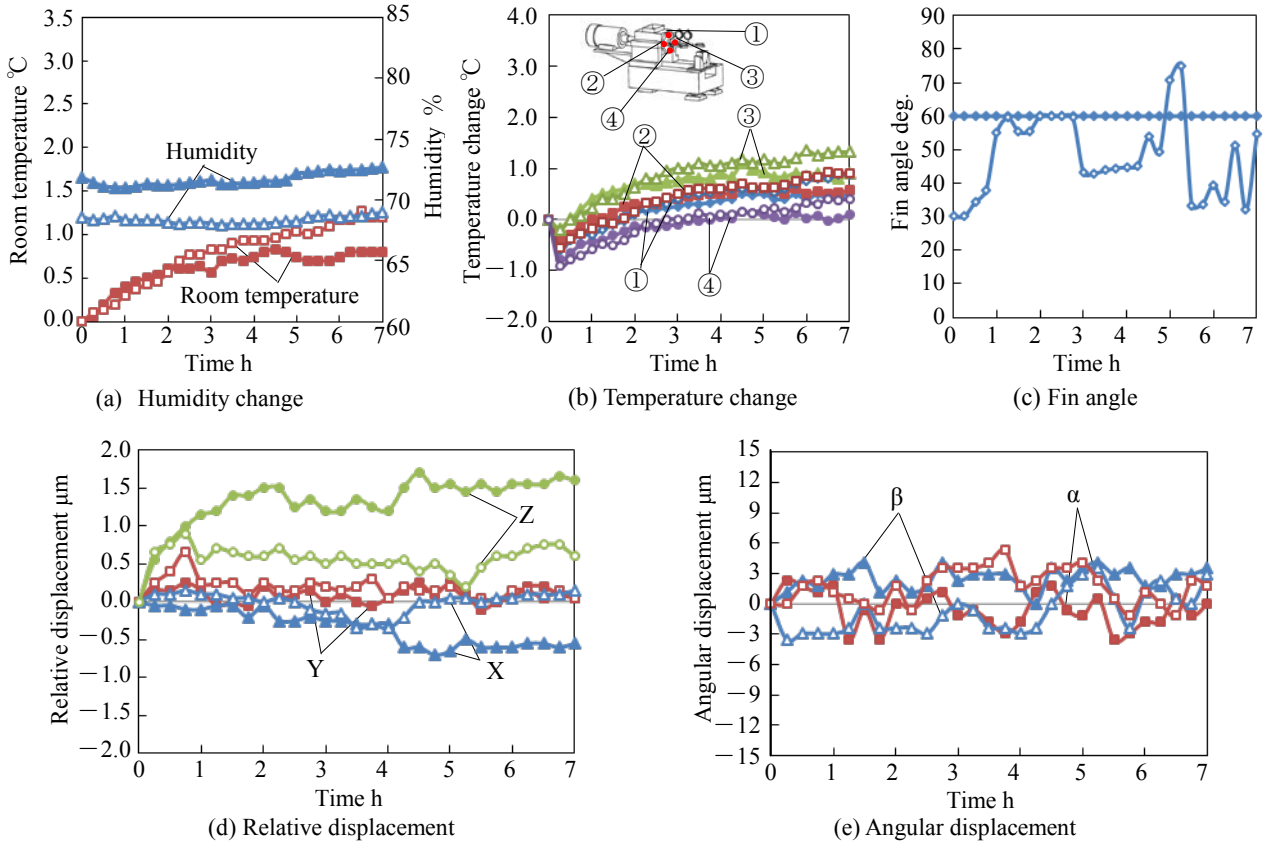

Fig.10 Bench lathe thermal deformation behavior under overcast weather conditions
(filled markers: without the proposed system; empty markers: with the proposed system)

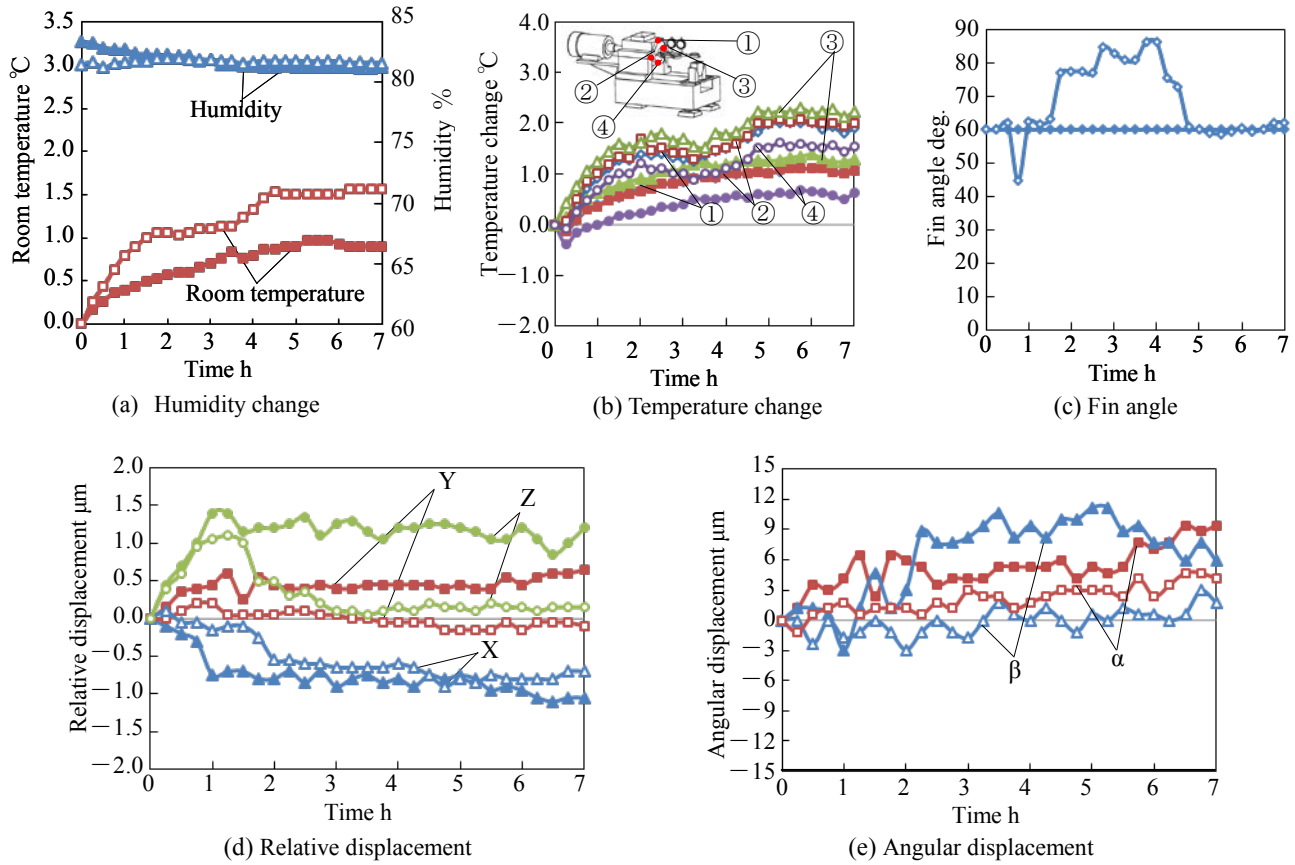

(a) Humidity change (b) Temperature change (c) Fin angle

(d) Relative displacement (e) Angular displacement

Fig.11 Bench lathe thermal deformation behavior under rainy weather conditions
(filled markers: without the proposed system; empty markers: with the proposed system)

IV. Evaluation of The Proposed Method Results

Finally, to evaluate the performance of the three countermeasures mentioned as a single method, experimentation on the bench lathe was done under three recreated weather conditions: fine, overcast and rainy. During experimentation, the spindle speeds varied according to case A on a no-cutting idling state and data was measured every 15 minutes; then, the optimum fin angle $\eta_o(t)$ at working time t was calculated on a personal computer, through the retrieved data and equation (2), to minimize thermal deformation $D_{kp}(t)$. Simultaneously, the optimum fin angle $\eta_o(t)$ was controlled through a feedforward control.

Moreover, other experiments that involved a 60 degrees fixed fin angle were also performed for comparison. In this regard, since there was just one bench lathe available, experimentation was performed at different times but with similar weather, humidity and room-temperature conditions.

Accordingly, experimental results under the fine, overcast and rainy weathers conditions are shown in Fig. 9, Fig. 10 and Fig. 11. Namely, the considered parameters were: (a) Humidity, (b) Temperature change, (c) Fin angle, (d) Relative displacement and (d) Angular displacement. In the three weather conditions, the bench lathe thermal deformations that resulted from the proposed method were smaller than in the case of the fixed fin angle experiments. Particularly, the relative displacements in all weather conditions were remarkably small: ΔX was 1.0 μm, ΔY was 1.0 μm and ΔZ was 1.1 μm. Since factories in general are subjected to diverse weather conditions, room-temperature or heat transfer rate change in an irregular and complex way. However, even under such circumstances, it is possible to calculate the optimum fin angle with this method. Therefore, the proposed method countermeasures are considered very effective. In addition, this method makes the improved technology an environmentally-friendly and affordable one by reducing parameters that involve higher costs.

V. Conclusions

From the experimental results it was concluded that:

1) Even though there was no active forced cooling, the thermal deformation of the bench lathe was considerably small

2) The air flow speed control used on the forced self-cooling system, through the neural network inverse analysis, was effective in achieving a stable operation, disregarding weather variations.

References

[1] Tanabe, I., Ikeda, S. and Urano, K., Estimation of optimum temperature for cooling oil on a spindle using inverse analysis of neural network (Effect of relearning), Transactions of Japan Society of Mechanical

Engineers, Series C, Vol. 69, No.679 (2003), pp. 819-824 (in Japanese).
[2] Kaneko, Y., Tanabe, I., Isobe, M. and Maeda, M., Development of a high precision lathe with countermeasure of environmental preservation for thermal deformation, Transactions of Japan Society of Mechanical Engineers, Series C, Vol. 70, No.700 (2004), pp. 3611-3616 (in Japanese).
[3] Tanabe, I., Ye, H. S., Iyama, T. and Abe, Y., Control of tool temperature using neural network for machining work-piece with low thermal conductivity, Transactions of Japan Society of Mechanical Engineers, Series C, Vol. 77, No.776 (2011), pp. 1556-1564 (in Japanese).
[4] Tanabe, I., Truong, H. M. and Yoshii, K., Turning with environment-friendly cooling method using water evaporation (1st report, Cooling effect of water evaporation and its applicability to tool tip cooling), Transactions of Japan Society of Mechanical Engineers, Series C, Vol. 66, No.643 (2000), pp. 1026-1030 (in Japanese).
[5] Tanabe, I., Matsushita, K. and Truong, H. M., Study on self-forced cooling for reducing thermal deformation of machine tool (Modeling of self-forced cooling and its applicability), Transactions of Japan Society of Mechanical Engineers, Series C, Vol. 67, No.660 (2001), pp. 2713-2718 (in Japanese).
[6] I. Tanabe and K. Yanagi, "A dual cooling jacket around spindle bearings with feed-forward temperature control system to decrease thermal deformation", JSME Int. J. Series C, Vol.39, No.1, (1996), pp149-155.
[7] I. Tanabe and K. Takada, "Thermal deformation of machine tool structure using resin concrete", JSME Int. J. Series C, Vol.39, No.1, (1994), pp384-389.
[8] D. E. Rumelhart, J. L. McClelland and the PDP research Group, "PARALLEL DISTRIBUTED PROCESSING",A Bradford Book, The MIT Press, Vol.1, (1986), pp318-361.
[9] Tanabe, I., Yamanaka, K., Mizutani, J. and Yamada, Y., A new design of lathe structure for reducing thermal deformation (Design of zero-center on three directions, self-compulsory cooling and design of thermal synchronism), Transactions of Japan Society of Mechanical Engineers, Series C, Vol. 65, No.639 (1999), pp. 4508-4513 (in Japanese).
[10] Tanabe, I., Ikariyama, T., Nishiyama, A. and Urano, K., Estimation of the most suitable temperature for cooling oil on a spindle using inverse analysis of nueral network, Transactions of Japan Society of Mechanical Engineers, Series C, Vol. 66, No.647 (2000b), pp. 2443-2448 (in Japanese).

I. TANABE Research assistant in 1982, Assistant professor in 1995 and Professor in 2005 in Nagaoka University of Technology. Research fields are machine tool, production engineering and processing study. Research themes are "Development of high speed polishing technology for complex die", "Development of cutting technology in strong alkaline water", "Development on simple lapping machine for machining mirror-like surface regarding die of cemented carbide", "New mirror-like finishing using the lathe with linear motor" and "Development of perfect simulation system on CAE using TAGUCHI-methods".